EUROPEAN ORGANIZATION FOR NUCLEAR RESEARCH

Proposal to the ISOLDE and Neutron Time-of-Flight Committee

MIRACLS at ISOLDE:
The Charge Radii of Exotic Magnesium Isotopes

May 13, 2020

M. Vilén[1], S. Malbrunot-Ettenauer[1], P. Fischer[2], H. Heylen[1], V. Lagaki[1,2], S. Lechner[1,4], F.M. Maier[1,2], W. Nörtershäuser[3], P. Plattner[1,5], S. Sels[1], L. Schweikhard[2], F. Wienholtz[3]

[1] *Experimental Physics Department, CERN, CH-1211 Geneva 23, Switzerland*
[2] *Institut für Physik, Universität Greifswald, D-17487 Greifswald, Germany*
[3] *Institut für Kernphysik, TU Darmstadt, D-64289 Darmstadt, Germany*
[4] *Technische Universität Wien, Karlsplatz 13, 1040 Wien, Austria*
[5] *University of Innsbruck, A-6020, Innrain 23, Austria*

Spokespersons and contact persons:
M. Vilén markus.kristian.vilen@cern.ch
S. Malbrunot-Ettenauer stephan.ettenauer@cern.ch

Abstract: The so-called island of inversion around neutron-rich magnesium isotopes represents a paradigmatic example of the 'collapse of the conventional shell-model ordering' [1] in atomic nuclei far away from stability. Understanding the underlying nuclear shell evolution from first principles remains a formidable task for contemporary nuclear theory. Building upon remarkable progress over the last years, ab-initio methods have begun to reach into this theoretically-demanding region of the nuclear chart, including the theoretical predication of electromagnetic ground-state properties of exotic radionuclides. Experimentally, these observables can be accessed by collinear laser spectroscopy (CLS) with high precision and accuracy and consequently serve as robust benchmarks for modern nuclear-structure calculations. As conventional, fluorescence-based CLS is limited in its experimental sensitivity, we propose new CLS measurements of exotic magnesium isotopes ($Z = 12$) by employing the novel, highly sensitive Multi Ion Reflection Apparatus for Collinear Laser Spectrosocpy (MIRACLS). Nuclear charge radii of ^{20,33,34}Mg will be determined to evaluate the predictive power of leading ab-initio methods spanning from the $N = 8$ shell closure in close proximity to the proton-drip line to neutron-rich nuclides, right in the centre of the island of inversion.

Requested shifts: 17 shifts (split into 2 runs over 1 year)

1 Physics Motivation

Ever since its discovery in the 1970s, through anomalous masses and spins in neutron-rich Na isotopes [2,3] as well as ^{32}Mg's ($Z = 12$, $N = 20$) low-lying 2^+-state [4], the island of inversion around $N = 20$ has been the focus of detailed studies in experimental and theoretical nuclear physics research (see [5] and references therein). Today, the experimental data is understood in terms of deformation and 2-particle-2-hole excitations between the normally occupied neutron $d_{3/2}$ orbit and 'intruding' $f_{7/2}$ and $p_{3/2}$ orbits. The associated disappearance of the $N = 20$ shell closure serves as a prime example of nuclear shell evolution far away from stability.

Theoretical work to describe the region in and around the island of inversion at $N = 20$ has been concentrated on shell-model approaches [6–9] and beyond mean field calculations [10,11]. However, a long-term goal of nuclear theory is the description of nuclear observables all across the nuclear chart, including the island of inversion, within one consistent framework. In this endeavour, ab initio methods play a central role by employing nuclear forces rooted through chiral effective field theory in the underlying quantum chromodynamics. Recent highlights of ab initio approaches include, among many others, the successful prediction of masses of neutron-rich Ca isotopes [12,13] and the calculation of the neutron and weak-charge distributions in ^{48}Ca providing a constraint on the radius of a neutron star [14]. Although ab initio calculations have extended all the way into the tin region around the $Z = 50$ shell closure [15,16], it is only now that the ab initio machinery debarks on the island of inversion around $N = 20$ [17,18]. Consequently, new experimental data will be of high demand in the near future to evaluate the predictions of these ongoing calculations. Since nuclear theory, including ab initio methods, have recently invested significant efforts into the description of electromagnetic ground-state properties such as nuclear charge radii, these observables are well suited as high-quality benchmarks [19–25].

Experimentally, root-mean-square (rms) charge radii of atomic nuclei, R_C, can be extracted with high precision and accuracy from high-resolution collinear laser spectroscopy (CLS) [26–28]. Previous laser-spectroscopy work in the region around the island of inversion covered Na [29] ($Z = 11$), Mg [30,31] ($Z = 12$), and Al isotopes [32] ($Z = 13$). Charge radii of Mg isotopes have been measured at COLLAPS and reveal a clear signature of the structural changes when entering into the region of deformation [33]. As displayed in Fig. 1a, these charge radii follow fairly linear trends between $A = 21 - 26$ and $A = 26 - 30$ in addition to a well-known odd-even staggering. At the shore of the island of inversion at ^{31}Mg ($N = 19$), the slope of the linear trend is suddenly increasing which signals the onset of deformation. To disentangle the odd-even staggering from the structural changes, differential mean-square radii are shown in Fig. 1b. Indeed, the filling of the respective neutron orbits is remarkably well imprinted onto the nuclear charge radii, including the intruder configuration for ^{31,32}Mg which marks the breakdown of the $N = 20$ shell closure. This surprisingly simple interpretation of the available experimental data raises clear expectations about the charge radii of the more neutron-rich Mg isotopes such as ^{33,34}Mg which are located well inside the island of inversion, as well as of ^{20}Mg at the robust $N = 8$ shell closure. Validating such extrapolations experimentally represents strong motivation for new CLS measurements on its own terms.
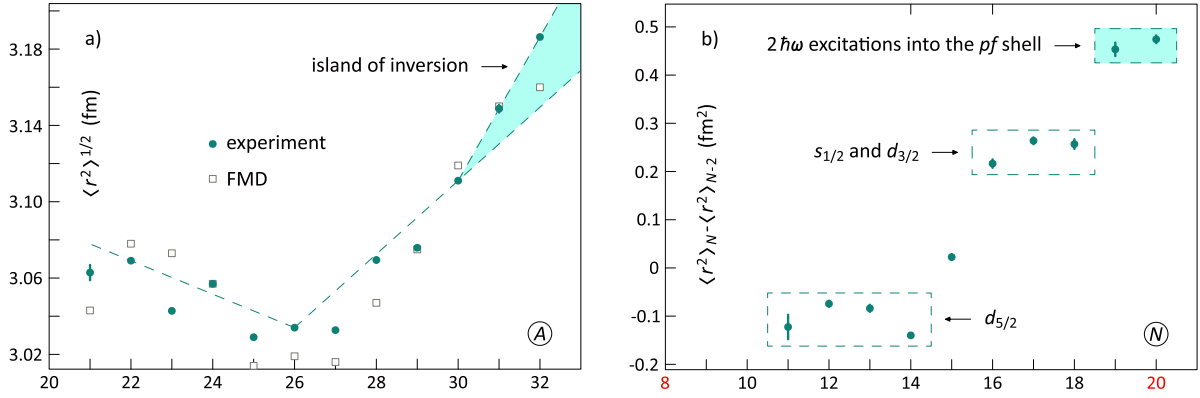
Figure 1: Experimental nuclear rms charge radii of magnesium isotopes in (a) and differential mean square radii in (b). (Correlated systematic uncertainties between charge radii are not shown). See text for details. Figures from [33].

Moreover, following the previous discussion on recent theoretical developments, leading ab initio methods are currently in the process of calculating charge radii along the entire Mg isotopic chain. In particular, these include coupled-cluster theory [18] and in-medium similarity renormalization group (VS-IMSRG) [34] which have been both very successful in the description of nuclear properties. Preliminary results for Mg charge radii from VS-IMSRG can be seen in Fig. 2. Since they are calculated using sd neutrons for $N < 20$ and pf neutrons for $N > 20$ nonphysical artifacts near $N = 20$ are to be expected and explain the large discontinuity at this mass. Ongoing VS-IMSRG work employs mixed-parity valence spaces. As demonstrated in [17] for other observables of nuclides in and around the island of inversion, this will make the transition across $N = 20$ more realistic. Above ^{32}Mg and all within the pf neutrons valence space, VS-IMSRG predicts a linear trend in the charge radii which is in line with the expectation from the experimentally measured charge radii. To confirm this prediction and benchmark these upcoming results of ab initio methods utilizing coupled-cluster theory and VS-IMSRG motivates our proposal for CLS measurements of ^{33,34}Mg.

On the neutron-deficient side of the isotopic chain, the experimental linear evolution in charge radii between $N = 9 - 14$ is well reproduced by VS-IMSRG although without a sizeable odd-even staggering. As far as ^{20}Mg is concerned, this preliminary VS-IMSRG predication also yields a larger charge radius compared to the neighbouring heavier Mg isotopes, as one may expect from the experimental trend and its interpretation discussed previously. However, in coupled-cluster theory (not shown here) the charge radius of ^{20}Mg is estimated to be notably lower compared to ^{22}Mg which is seen as a consequence of its $N = 8$ magicity [18]. Indeed, a stabilizing effect at a magic neutron number manifesting itself in a (relative) decrease of the nuclear charge radius at the shell closure is commonly observed all across the nuclear chart. For $N = 8$, this is in fact the case for the Ne isotopes [35] and possibly also for Na isotopes [29]. For the latter, a decrease is found for ^{21}Na, one nuclide away from the shell closure with an experimentally still unknown R_C. These differences in expectations for the charge radius of ^{20}Mg in different theoretical calculations as well as in experimental systematics can only be resolved by new experimental
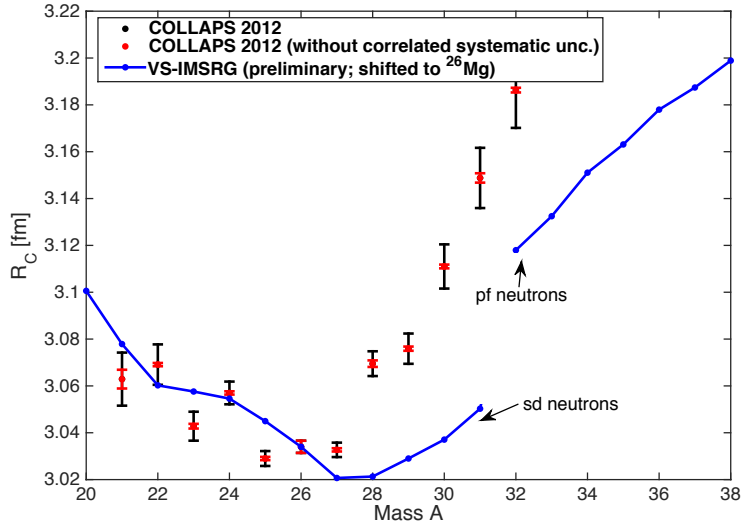
3

Figure 2: Experimental nuclear rms charge radii of magnesium isotopes in [33] compared to preliminary results of VS-IMSRG [34]. The latter are shifted by a constant offset of 0.155 fm to match the experimental value of ^{26}Mg. See text for details.

data, which motivates our present proposal to reach ^{20}Mg, as well.

In summary, we propose measurements of the nuclear charge radii of ^{20,33,34}Mg in order to provide solid experimental data from the $N = 8$ shell closure all the way into the centre of the island of inversion around $N = 20$. These data will serve as high-quality benchmarks for novel theoretical approaches which for the first time extend their reach into the island of inversion with ab initio methods. As such, this proposal represents an intriguing case where the forefront of nuclear theory and experiment both reach out together to access new territory (in terms of nuclear charge radii). To achieve this goal, the novel Multi Ion Reflection Apparatus for Collinear Laser Spectroscopy (MIRACLS) will be employed in order to match the experimental sensitivity of high-resolution laser spectroscopy to the low yields of these exotic Mg nuclides.

2 Experimental method

As explained in details in our previous INTC reports (INTC-I-197, INTC-I-215, and INTC-M-019), MIRACLS is designed to perform collinear laser spectroscopy in a Multi-Reflection Time-of-Flight (MR-ToF) device. When the trapped ion bunch of exotic radionuclides is probed by a spectroscopy laser during each ion revolution in the MR-ToF instrument, the experimental sensitivity is greatly increased compared to conventional, single-pass CLS. Hence, radionuclides previously out of reach due to their low production yields at ISOLDE will become accessible by MIRACLS. Although we have successfully demonstrated first work towards more common ionic systems, Mg$^+$ ions represent the ideal first science application of MIRACLS as their ionic structure represents a closed two-level system. Thus, laser-excited ions decay back into their initial fine-structure state and can, for nuclides with spin 0 such as ^{20,34}Mg, be probed many times until they undergo radioactive decay.
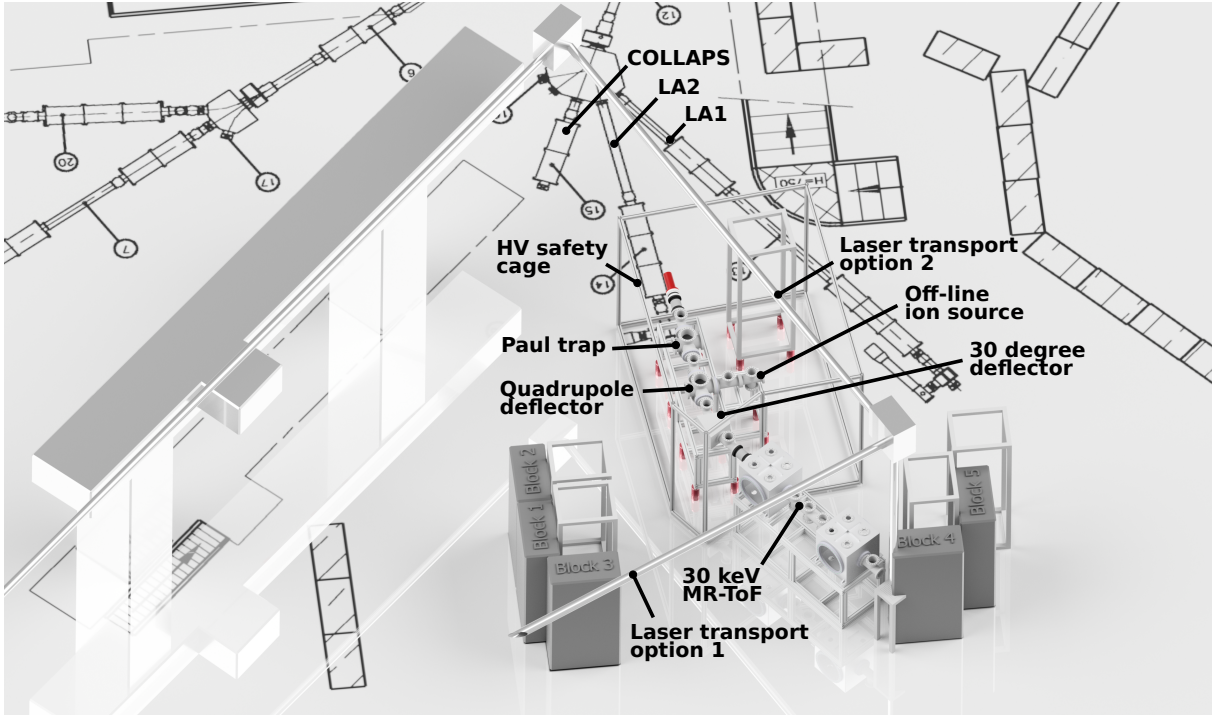
4

Figure 3: A compact MIRACLS at the LA2 beam line at ISOLDE. The COLLAPS beam line is only partially shown here. See text for details.

An initial, compact MIRACLS configuration

As introduced in our earlier report INTC-M-019, MIRACLS utilizes a combination of a cryogenic Paul trap and an MR-ToF device operating at ion beam energies of $\geq 30\,\text{keV}$. Our preferred location in the ISOLDE hall remains the area next to the ISOLDE Decay Station (IDS) currently occupied by the Nicole set-up. This area provides sufficient space for MIRACLS to be implemented in its full configuration that will allow us to fully take advantage of MIRACLS' unique science potential, including the preparation of high-quality radioactive ion beams to downstream experiments such as PUMA.

However, the exceptional measures to fight the global COVID-19 epidemic severely impact our project schedule. To achieve the science goals of our ERC project in the remaining funding period despite this external challenge, we have adopted an alternative, more compact MIRACLS design. Although significantly less versatile and powerful compared to the complete apparatus, it is tailored to our very first science cases, thus, reducing the set-up's overall complexity, e.g. by falling back to a room-temperature Paul trap. Moreover, it re-integrates existing (low-energy) beamline sections of our proof-of-principle experiment, which minimizes the remaining construction work.

Our envisioned location for the new system design is the LA2 beam line which offers us two benefits: Currently the area next to IDS is still occupied by the Nicole set-up. Constructing MIRACLS at LA2 will allow us to proceed without the need to wait for Nicole to be removed. The second benefit to commissioning MIRACLS at LA2 is the relative simplicity of constructing the necessary infrastructure for transporting laser light to the MR-ToF device. At LA2 much of the infrastructure is already available as a result of

the close proximity of the COLLAPS system. The compact MIRACLS set-up is presented in Fig. 3, along with tentative solutions for the laser-light transport to MIRACLS.

The amount of space available at LA2 necessitates making several changes to the Paul trap, the off-line ion source and the connecting beam lines. Equipment needed for a cryogenic Paul trap would require more floor space than is available at LA2 and it would significantly increase the technical complexity of the system. Therefore, a simple room-temperature Paul trap will be constructed. Space limitations also lead us to change the positioning of the off-line ion source and to use more compact, simplified ion optics at the expense of reduced beam tuning possibilities. For example, asymmetrical ion beam focusing downstream of the 30° deflector would require a more complex system.

At LA2, the Paul trap will be directly connected to the ISOLDE beam line. The off-line ion source will be operated downstream of the Paul trap on a shared high voltage platform. The two will be connected with a low energy beam line (2 kV below the main HV level) utilizing a quadrupole deflector, together with Einzel lenses and steering optics. In this configuration some ion optical elements will be common to ion beams being injected to and extracted from the Paul trap. Fast high-voltage switches will be used to change the voltages applied to the ion optics based on the direction of the ion beam. The benefit of such a system is that for the price of a more complex tuning process we will need a smaller total number of focusing and steering elements, resulting in a more compact system. Ion bunches of 2-keV beam energy from the Paul trap will pass through a 30° deflector and subsequently be accelerated to 50 keV. The deflector will provide the necessary laser access to the MR-ToF device where the ion bunches will be trapped for CLS measurements. The entire ion optics has been validated in detailed simulations of ion trajectories throughout this compact MIRACLS system.

The MR-ToF device itself will be built in its optimal configuration, thus, according to its original design meant for the area next to IDS. When MIRACLS will be relocated to the larger area the MR-ToF device will be transported to the new beam line and recommissioned without modifications. However, almost all other parts of the system will need to be modified at that time for the system to reach its originally intended performance.

In summary, the compact MIRACLS system at LA2 will be modified in a way that sacrifices the cryogenic operation of the Paul trap, the upstream off-line ion source operated at 50 keV, the ion beam transport between the Paul trap and MR-ToF device at 50 keV, the ion optics optimized for beam quality instead of space and the possibility of providing ion beams to downstream users. However, the compact system design will allow us to reach the physics goals set out in our ERC project. Once these goals are achieved, we intend to relocate the MR-ToF device and couple it to a cryogenic Paul trap and beam lines optimized for 50 keV transfer energy. This final configuration will allow us to lead MIRACLS to is full scientific potential.

Required resources

Resources required for constructing, commissioning and operating MIRACLS at LA2 closely follow the requirements in our previous reports INTC-M-019 and INTC-I-215, with some modifications due to the compact system design. Total power requirement will be lower without the need for a cryocooler and a chiller. We estimate a maximum peak

consumption of 80 kW. However, even with the lower requirement additional electrical installations will be needed in order to guarantee sufficient power availability to travelling set-ups coupled to LA1. An additional laser transport system will be required, as shown in Fig. 3. Cooling water from ISOLDE will not be required with the compact system. Changes to the positioning on existing concrete blocks in the ISOLDE hall will be necessary. Block 4 presented in Fig. 3 will have to be moved to the right in order to make enough space for the laser transport system. This block is currently used as a mounting point for various pieces of infrastructure, such as electrical installations and a radiation monitor. Additionally, we request block 5 to be removed. Discussions about further details about the integration of the compact MIRACLS design are currently ongoing with ISOLDE operation team as well as the COLLAPS collaboration.

3   Beamtime request

For the production of neutron-rich Mg isotopes a UC target promises the highest yields with minimal isobaric contamination. Previously measured yields with RILIS account for 3000 ions/μC for ^{33}Mg and 140 ions/μC for ^{34}Mg, respectively. For ^{20}Mg the preferred ISOLDE target is a SiC sub-micron target for which a yield of 15000 ions/μC has been measured for ^{21}Mg. Calculated production yields in FLUKA and ABRABLA predict a reduction in in-target yield from ^{21}Mg to ^{20}Mg by a factor of 26 and 15, respectively. Given that the half-lives of both isotopes are similar, 120 ms and 91 ms, respectively, an additional loss in yield during the release from the target should be rather small. Hence, a ^{20}Mg yield in the order of 500 ions/μC can be expected. Overwhelming contamination of neutron-deficient Na isotopes is a major concern for proton-rich Mg isotopes. The use of LIST for Na suppression will hence be of major importance. LIST can reduce the amount of Na by up to 6 orders of magnitude but will also reduce the Mg yield by factor of up to 30 [36]. This results in an expected yield of about 17 ions/μC for ^{20}Mg.

The beamtime request is based on the performance of the successful MIRACLS proof-of-principle experiment [37–40]. Its (preliminary) sensitivity is shown in Fig. 4 along with an extrapolation to the 30-keV set-up. This extrapolation is exclusively based on the number of photon detectors and the expected reduction in laser-stray light as typically achieved in an identical optical detection region at COLLAPS. It does, however, not include differences in the FWHM of the laser spectroscopic line shape or in the efficiency of ion trapping, storage or laser-excitation in the 30-keV MR-ToF device. All of these should be more favourable in the 30-keV set-up. Although MIRACLS will enhance the sensitivity for ^{33}Mg, too, optical pumping to other hyperfine states will eventually diminish the CLS signal for this nuclide. However, the initial larger yield is expected to compensate the relative reduction in sensitivity.

Based on the yield estimate and assumed ion-transfer efficiencies of ISCOOL, the ISOLDE beamline, as well as the MIRACLS system, the number of ions injected into the MR-ToF device is determined. Taking into account the expected experimental CLS sensitivity of Fig. 4, the number of frequency scans is calculated to obtain a signal-to-noise ratio of at least S/N=5. For each isotope of interest we aim for at least 5 independent measurement runs under varying conditions such as different trapping time. Additional time
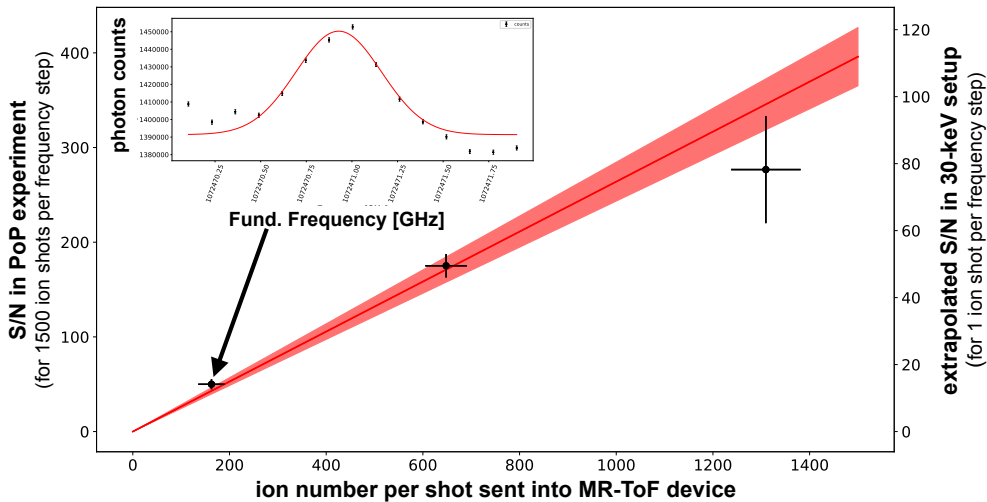
7

Figure 4: Experimental CLS sensitivity expressed in terms of signal-to-noise ratio (S/N) for $^{24}Mg^+$ ions trapped for 1500 revolutions inside MR-ToF device of the MIRACLS proof-of-principle (PoP) experiment. The insert shows a typical resonance for $^{24}Mg^+$. A simple extrapolation of the sensitivity for the 30-keV apparatus is given on the right y-axis assuming a single ion shot per freqency step. See text for details.

is reserved for initial frequency scans to locate the position of the CLS resonance, for reference measurements with a stable Mg isotope, as well as for cycling the magnets of the mass separator. Hence, for a UC target we request 2 8-hour shifts for ^{34}Mg, 3 shifts for ^{33}Mg, as well as 2 shifts for $^{28-32}Mg$. The latter will serve as a benchmark for systematic uncertainties under online conditions which are imperative when establishing a novel technique. For the SiC sub-micron target we request 5 shifts for ^{20}Mg and 1 shift for studies of systematic uncertainties. ^{20}Mg's much longer half-life compared to ^{34}Mg enables a longer storage time at MIRACLS and partially compensates for the lower yield. For each target, we will require a setup time with stable Mg beam over 2 shifts.

As already stressed in our previous reports, availability of stable beam during LS2 to establish the ion transfer from ISOLDE to MIRACLS is of utmost importance for the success of the MIRACLS project.

We note in passing that a future upgrade in proton energy and intensity promises a significant increase in the yields of neutron-rich Mg isotopes. This prospect would motivate a future MIRACLS proposal on $^{35,36}Mg$.

Summary of requested shifts: 17 shifts split into 2 runs

References

[1] B. H. Wildenthal et al. Collapse of the conventional shell-model ordering in the very-neutron-rich isotopes of Na and Mg. *Phys. Rev. C*, 22:2260–2262, Nov 1980.

[2] C. Thibault, et al. Direct measurement of the masses of ^{11}Li and $^{26-32}Na$ with an on-line mass spectrometer. *Phys. Rev. C*, 12:644–657, Aug 1975.

[3] G. Huber, et al. Spins, magnetic moments, and isotope shifts of $^{21-31}$Na by high resolution laser spectroscopy of the atomic D_1 line. *Phys. Rev. C*, 18:2342–2354, Nov 1978.

[4] C. Détraz, et al. Beta decay of $^{27-32}$Na and their descendants. *Phys. Rev. C*, 19:164–176, Jan 1979.

[5] T. Otsuka, et al. Evolution of shell structure in exotic nuclei. *Rev. Mod. Phys.*, 92:015002, Mar 2020.

[6] Y. Utsuno, et al. Varying shell gap and deformation in $N \sim 20$ unstable nuclei studied by the Monte Carlo shell model. *Phys. Rev. C*, 60:054315, Oct 1999.

[7] T. Otsuka, et al. Monte Carlo shell model for atomic nuclei. *Progress in Particle and Nuclear Physics*, 47(1):319 – 400, 2001.

[8] E. Caurier, et al. Merging of the islands of inversion at $N = 20$ and $N = 28$. *Phys. Rev. C*, 90:014302, Jul 2014.

[9] N. Tsunoda, et al. Exotic neutron-rich medium-mass nuclei with realistic nuclear forces. *Phys. Rev. C*, 95:021304, Feb 2017.

[10] P.-G. Reinhard, et al. Shape coexistence and the effective nucleon-nucleon interaction. *Phys. Rev. C*, 60:014316, Jun 1999.

[11] J. Terasaki, et al. Deformation of nuclei close to the two-neutron drip line in the Mg region. *Nuclear Physics A*, 621(3):706 – 718, 1997.

[12] A. T. Gallant, et al. New Precision Mass Measurements of Neutron-Rich Calcium and Potassium Isotopes and Three-Nucleon Forces. *Phys. Rev. Lett.*, 109:032506, Jul 2012.

[13] F. Wienholtz, et al. Masses of exotic calcium isotopes pin down nuclear forces. *Nature*, 498(7454):346–349, 2013.

[14] G. Hagen, et al. Neutron and weak-charge distributions of the 48Ca nucleus. *Nature Physics*, 12(2):186–190, 2016.

[15] T. D. Morris, et al. Structure of the Lightest Tin Isotopes. *Phys. Rev. Lett.*, 120:152503, Apr 2018.

[16] V. Manea, et al. First Glimpse of the $N = 82$ Shell Closure below $Z = 50$ from Masses of Neutron-Rich Cadmium Isotopes and Isomers. *Phys. Rev. Lett.*, 124:092502, Mar 2020.

[17] T. Miyagi, et al. Ab initio multi-shell valence-space Hamiltonians and the island of inversion. Unpublished, arXiv:2004.12969, 2020.

[18] G. Hagen. 2020. private communications.

[19] R. F. Garcia Ruiz, et al. Unexpectedly large charge radii of neutron-rich calcium isotopes. *Nature Physics*, 12(6):594–598, 2016.

[20] P.-G. Reinhard et al. Toward a global description of nuclear charge radii: Exploring the Fayans energy density functional. *Phys. Rev. C*, 95:064328, Jun 2017.

[21] A. J. Miller, et al. Proton superfluidity and charge radii in proton-rich calcium isotopes. *Nature Physics*, 15(5):432–436, 2019.

[22] M. Hammen, et al. From Calcium to Cadmium: Testing the Pairing Functional through Charge Radii Measurements of $^{100-130}$Cd. *Phys. Rev. Lett.*, 121:102501, Sep 2018.

[23] C. Gorges, et al. Laser Spectroscopy of Neutron-Rich Tin Isotopes: A Discontinuity in Charge Radii across the $N = 82$ Shell Closure. *Phys. Rev. Lett.*, 122:192502, May 2019.

[24] S. Kaufmann, et al. Charge Radius of the Short-Lived ^{68}Ni and Correlation with the Dipole Polarizability. *Phys. Rev. Lett.*, 124:132502, Apr 2020.

[25] R. P. de Groote, et al. Measurement and microscopic description of odd–even staggering of charge radii of exotic copper isotopes. *Nature Physics*, 2020.

[26] K. Blaum, et al. Precision atomic physics techniques for nuclear physics with radioactive beams. *Physica Scripta*, 2013(T152):014017, 2013.

[27] P. Campbell, et al. Laser spectroscopy for nuclear structure physics. *Progress in Particle and Nuclear Physics*, 86:127 – 180, 2016.

[28] R Neugart et al. Collinear laser spectroscopy at ISOLDE: new methods and highlights. *J. Phys. G: Nucl. Part. Phys*, 44:064002, 2017.

[29] G. Torbohm, et al. State-dependent volume isotope shifts of low-lying states of group-IIa and -IIb elements. *Phys. Rev. A*, 31:2038–2053, Apr 1985.

[30] G. Neyens, et al. Measurement of the Spin and Magnetic Moment of ^{31}Mg: Evidence for a Strongly Deformed Intruder Ground State. *Phys. Rev. Lett.*, 94:022501, Jan 2005.

[31] D. T. Yordanov, et al. Spin and Magnetic Moment of ^{33}Mg: Evidence for a Negative-Parity Intruder Ground State. *Phys. Rev. Lett.*, 99:212501, Nov 2007.

[32] H. Heylen et al. in preparation.

[33] D. T. Yordanov, et al. Nuclear Charge Radii of $^{21-32}$Mg. *Phys. Rev. Lett.*, 108:042504, Jan 2012.

[34] J. D. Holt et al. private communications, 2020.

[35] W. Geithner, et al. Masses and Charge Radii of $^{17-22}$Ne and the Two-Proton-Halo Candidate ^{17}Ne. *Phys. Rev. Lett.*, 101:252502, Dec 2008.

[36] S. Rothe et al. private communications, 2020.

[37] F. M. Maier, et al. Simulations of a proof-of-principle experiment for collinear laser spectroscopy within a multi-reflection time-of-flight device. *Hyperfine Interactions*, 240(1):54, 2019.

[38] S. Lechner, et al. Fluorescence detection as a new diagnostics tool for electrostatic ion beam traps. *Hyperfine Interactions*, 240(1):95, 2019.

[39] S. Sels, et al. First steps in the development of the Multi Ion Reflection Apparatus for Collinear Laser Spectroscopy. *Nuclear Instruments and Methods in Physics Research Section B: Beam Interactions with Materials and Atoms*, 463:310 – 314, 2020.

[40] V. Lagaki, et al. Stray-light suppression for the MIRACLS proof-of-principle experiment. *Acta Physica Polonica B*, 51:571–576, (2020).

Appendix

DESCRIPTION OF THE PROPOSED EXPERIMENT
The experimental set-up comprises: *MIRACLS (at LA2)*

Part of the	Availability	Design and manufacturing
MIRACLS at LA2	Existing	⊠ CERN/collaboration responsible for the design and manufacturing
[insert lines if needed]		

HAZARDS GENERATED BY THE EXPERIMENT
All hazards involving the MIRACLS installation at LA2 will be discussed with the CERN safety team as part of MIRACLS integration plan into the ISOLDE hall. Upon installation, all safety documents will be completed in close collaboration with the CERN safety team. This will be done much in advance of the first online beamtime.